Teknomekanik, Vol. 9, No. 3, 2026, pp. 378-395
e-ISSN: 2621-8720 p-ISSN: 2621-9980

Combustion and emission responses of methanol-enriched catalytic plastic waste pyrolysis oil in a stationary otto engine

Enzo Wiranta Battra Siahaan[1,2], Tulus Burhanuddin Sitorus[1*], Himsar Ambarita[1], Taufiq Bin Nur[1], Ilmi Abdullah[1], Janter P. Simanjuntak[3]

[1] Department of Mechanical Engineering, Faculty of Engineering, Universitas Sumatera Utara, **Indonesia**
[2] Department of Mechanical Engineering, Faculty of Engineering, Universitas HKBP Nommensen, **Indonesia**
[3] Department of Mechanical Engineering, Faculty of Engineering, Universitas Negeri Medan, **Indonesia**

[*]Corresponding Author: tulus.burhanuddin@usu.ac.id
Received: 28 April 2026; *Revised:* 09 October 2026; *Accepted:* 16 October 2026

Cite this https://doi.org/10.24036/teknomekanik.v9i3.56972

Abstract: Plastic waste pyrolysis oil (PWPO) offers a waste-to-energy pathway; however, its use in small spark-ignition engines is constrained by fuel-property variability, mixture preparation, and combustion phasing. This study integrated evidence on fuel properties, crank-angle-resolved combustion, indicated performance, cyclic variability, and emissions for PWPO produced using a silica-alumina catalyst containing 0, 5, 10, and 15 vol.% methanol in a 163 cm³ single-cylinder stationary Otto engine at engine speeds of 1,500–4,000 rpm. A 4 × 6 operating matrix was used to compare pressure-volume behavior, pressure-crank-angle development, apparent heat-release rate (HRR), CA10/CA50/CA90 phasing, net indicated mean effective pressure ($IMEP_n$), COVIMEP, and gaseous emissions. The response to methanol was distinctly non-monotonic. M10 generally produced the highest $IMEP_n$, whereas M5 yielded the lowest speed-averaged CO (3.87 vol.%, 16.9% below PWPO) and M10 yielded the lowest speed-averaged HC (411.7 ppm, 28.1% below PWPO); CO emissions from M10 were 14.2% lower than those from PWPO. Re-examination of the archived burn-phasing data showed that the M10 CA10-CA90 interval was approximately 2.8-5.6% longer than that of PWPO despite earlier CA90, while M10 COVIMEP remained approximately 16-25% under no-load conditions. The evidence therefore supports a trade-off between fuel composition and engine responses rather than a concentration-proportional benefit or statistically validated optimum: moderate methanol reformulation improved pressure development and incomplete-combustion emissions, but did not eliminate cyclic instability.

Keywords: catalytic plastic waste pyrolysis oil; crank-angle pressure; heat-release rate; methanol reformulation; stationary otto engine

© The Author(s)
Published by Universitas Negeri Padang.
This is an open-access article under the: https://creativecommons.org/licenses/by/4.0/

1. Introduction

Plastic waste accumulation presents persistent waste-management and environmental challenges [1], [2]. Pyrolysis can convert polyolefin-rich waste into liquid products, gas, and char under oxygen-limited conditions, coupling waste reduction with energy recovery [3], [4]. The liquid fraction can have an engine-relevant heating value, but its composition and volatility remain strongly dependent on the feedstock, reactor conditions, catalyst, and condensation strategy.

Direct use of PWPO in spark-ignition (SI) engines remains challenging because it is a chemically complex, composition-sensitive fuel rather than a narrowly specified gasoline surrogate. A plausible working hypothesis is that the coexistence of lighter and heavier hydrocarbon fractions, together

with variations in viscosity and volatility, produces non-uniform vaporization and locally fuel-rich regions in a carbureted intake system. These effects can slow flame-kernel growth, broaden cycle-to-cycle phasing, and increase CO and unburned HC emissions when late-vaporizing material does not oxidize completely [5], [6], [7], [8], [9], [10]. This hypothesis is treated as mechanistic interpretation rather than direct demonstration based on compositional measurements, because the present engine dataset does not contain quantitative GC-MS peak fractions for causal attribution.

Methanol provides a complementary reformulation route because its fuel-bound oxygen, high octane rating, and potential favorable laminar burning characteristics can support oxidation and flame development [11], [12], [13]. Its thermophysical effects are not uniformly beneficial: the high latent heat of vaporization can cool the charge and alter overall combustion phasing, especially at low load or high methanol fractions [14], [15]. Accordingly, methanol content must be assessed through coupled fuel-property, combustion, stability, and emission responses rather than through a single performance indicator.

An additional constraint is phase compatibility. Methanol is strongly polar, whereas most fuel-range hydrocarbons in PWPO are comparatively non-polar, so single-phase behavior cannot be assumed a priori. Previous work, likewise indicates that alcohol-hydrocarbon miscibility depends on blend composition, temperature, water content, and the presence of intermediate-polarity species [16]. In the present work, M5, M10, and M15 were mixed using a magnetic stirrer at ambient conditions and inspected for visible separation immediately before testing. No data from long-duration storage or phase-envelope testing were archived; the blends are therefore described only as visually homogeneous test mixtures and should not be taken as evidence of thermodynamic miscibility.

Three relevant research streams have rarely been examined together. PWPO studies have predominantly addressed pyrolysis yield, physicochemical characterization, or basic engine feasibility [6], [7], [8]; methanol-fueled SI-engine studies have largely examined gasoline-based or other conventional fuel systems and different engine architectures [11], [12]; and RSM/desirability methods are already established for engine optimization [17], [18]. The unresolved question is therefore not whether PWPO can be produced, whether methanol can alter SI-engine combustion, or whether RSM can be applied. Rather, it is whether methanol-induced property changes in catalyst-derived PWPO produce coordinated or competing changes in combustion phasing, apparent HRR, indicated work, cyclic variability, and incomplete-combustion emissions in a small stationary engine, and whether those responses remain monotonic as methanol concentration increases. Within the literature set reviewed for this study, these responses have not been evaluated together for a catalytic PWPO-methanol matrix under one crank-angle-resolved stationary-engine experiment. Accordingly, the novelty is the integrated evidence chain from fuel properties to pressure/HRR development, CA10-CA90 phasing, $IMEP_n$, COVIMEP, and CO/HC response, with particular emphasis on the observed non-monotonic methanol effect. RSM is not claimed as a novelty, and all conclusions are bounded to the measured 0-15 vol.% methanol range, 1,500-4,000 rpm sweep, and no-load configuration.

Silica-alumina was selected as an acidic cracking catalyst; its use was informed by prior work on silica-alumina chemistry in other conversion systems [19]. Its effects on plastic cracking, liquid-fuel composition, and engine response were not evaluated in this study. The retained experimental package, however, identifies the catalyst only as silica-alumina and does not preserve its Si/Al ratio, BET surface area, acidity distribution, particle size, catalyst-to-feed ratio, or regeneration history. Consequently, catalyst chemistry is treated here as a process descriptor rather than an independently optimized variable, and no causal attribution is made to a specific catalyst property.

Although the engine is intended for stationary service, the 1,500 - 4,000 rpm sweep was used to characterize speed-dependent sensitivity, not to simulate continuous variable-speed generator

© The Author(s)
Published by Universitas Negeri Padang.
This is an open-access article under the: https://creativecommons.org/licenses/by/4.0/

operation. Small mechanically governed utility engines can be operated at different governed set points during characterization; the sweep allows methanol-speed interactions to be resolved and identifies a candidate operating region. Any deployment conclusion must therefore be confirmed at the required constant governed speed and load.

2. Material and methods

2.1 Material

The reported plastic feedstock included LDPE, HDPE, PP, and PS, but polymer-specific proportions were not documented in the retained study materials. Accordingly, no constituent is identified as dominant. Published work indicates that pyrolysis-product characteristics depend on polymer type [7]. Silica-alumina was used in the reported cracking step, without a comparative assessment of its influence on the recovered fuel.

2.2 Experimental apparatus and fuel preparation

The reported process involved a laboratory-scale fixed-bed pyrolysis reactor, from which the condensable liquid was recovered as PWPO. Reactor-atmosphere controls were not documented in the retained material; oxygen exclusion is therefore not asserted as a verified test condition. The available documentation contains no original GC-MS chromatograms, FTIR spectra, analytical protocols, or identification reports; consequently, the performance of those analyses and any species-level or functional-group assignments cannot be independently established. No quantitative fuel-composition results are inferred. PWPO was blended with methanol at 5, 10, and 15 vol.% (M5, M10, and M15) by magnetic stirring at ambient conditions and was used only when visual inspection showed no macroscopic separation. The retained records do not preserve the pyrolysis thermal history, residence time, catalyst-to-feed ratio, methanol purity, or magnetic-stirring speed and duration. These details are therefore acknowledged as reproducibility limitations rather than inferred. Table 4 reproduces the nominal standards listed in the fuel-property summary: SNI 3506:2017 for density, kinematic viscosity, initial boiling point, and flash point; ASTM D4809-06 for gross (higher) heating value; and ASTM D2699 for research octane number. These method-property assignments have not been independently checked against original laboratory reports; their applicability, test conditions, and measurement uncertainties therefore require author verification.

2.3 Experimental procedure and test conditions

Each fuel (PWPO, M5, M10, and M15) was tested independently after the fuel system had been purged. The single-cylinder carbureted Otto engine was operated under steady-state no-load at 1,500; 2,000; 2,500; 3,000; 3,500; and 4,000 rpm after thermal stabilization. In-cylinder pressure and crank-angle signals were acquired synchronously, while CO, HC, CO_2, O_2, λ, and AFR were recorded from the exhaust stream. The retained test archive does not preserve the exact stabilization criterion, run-order randomization, number of independent engine-test repetitions, or number of cycles contributing to each reported averaged combustion trace. Accordingly, repeat-run standard deviations and confidence intervals cannot be reported, and the speed sweep is interpreted as a characterization matrix rather than as continuous stationary-generator duty. Table 1 summarizes the engine and operating range; Figure 1 and Table 2 document the available measurement chain and instrument record.

Figure 1 illustrates fuel preparation and delivery, the Kistler 6118C in-cylinder pressure transducer, Kistler 2614D11 crank-angle encoder, exhaust sampling probe, EPSG4 gas analyzer, synchronized KiBox acquisition, and subsequent data reduction. No load-absorbing device was included because the reported tests were steady-state no-load.

© The Author(s)
Published by Universitas Negeri Padang.
This is an open-access article under the: https://creativecommons.org/licenses/by/4.0/

Table 1. Key engine specifications and tested operating range

Parameter	Specification
Engine / configuration	Honda GX160-type; single-cylinder, four-stroke SI
Fuel metering	Conventional carburetor
Displacement	163 cm³
Bore × stroke	68 × 45 mm
Compression ratio	8.5:1
Ignition	Transistorized magneto
Rated power	5.5 hp
Maximum torque	10.3 N·m at 2,500 rpm
Governor	Mechanical
Tested speeds	1,500-4,000 rpm; 500-rpm interval
Test mode	Steady-state, no-load characterization

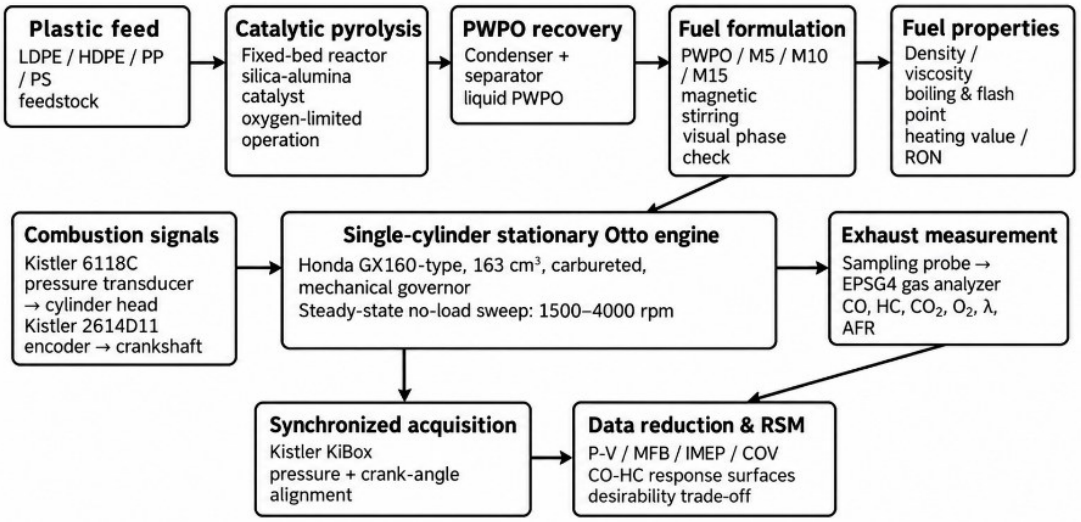


Figure 1. Experimental apparatus and synchronized data-acquisition workflow

Table 2. Measurement instrumentation reported for the engine test platform

Measured quantity	Instrument / model	Reported range / capability	Reporting note
Cylinder pressure	Kistler 6118C spark-plug pressure transducer	0-200 bar	Sensitivity/calibration certificate governs uncertainty.
Crank angle / speed	Kistler 2614D11 encoder	0–12,000 rpm	Angular resolution and TDC referencing were not archived.
Synchronized acquisition	Kistler KiBox combustion analyzer	Pressure-crank-angle acquisition	Sampling/filter settings were not archived.
CO	EPSG4 gas analyzer	0-10 vol.%	Calibration-gas record/uncertainty not archived.

© The Author(s)
Published by Universitas Negeri Padang.
This is an open-access article under the: https://creativecommons.org/licenses/by/4.0/

Measured quantity	Instrument / model	Reported range / capability	Reporting note
HC	EPSG4 gas analyzer	0-9999 ppm	HC reporting basis should follow the instrument certificate.
CO_2	EPSG4 gas analyzer	0-20 vol.%	Calibration-gas record/uncertainty not archived.
O_2 / λ / AFR	EPSG4 gas analyzer	λ: 0-2.000; other ranges not documented	Dry/wet basis and uncertainty were not archived.

2.4 Data reduction and statistical scope

Data reduction distinguished measured quantities from derived responses. Net indicated work and net indicated mean effective pressure were obtained from the cylinder pressure-volume loop as $W_{i,n} = \oint p\, dV$ and $IMEP_n = W_{i,n}/Vd$. Cycle variability was expressed as COVIMEP = 100(σIMEP/mean IMEP), and burn duration as BD = CA90 − CA10. In the archived mass-fraction-burn plots, CA10, CA50, and CA90 denote the crank angles at which the cumulative burned fraction reaches 10%, 50%, and 90%, respectively. Because the raw cycle files and the original processing settings are unavailable, these phasing markers are reported as archived derived quantities and are not independently recalculated. COVIMEP is likewise interpreted as within-run cyclic dispersion from the archived combustion analysis, not as a substitute for between-run experimental repeatability.

The apparent net heat-release rate follows the single-zone first-law form $dQ_n/d\theta = [\gamma/(\gamma-1)]p(dV/d\theta) + [1/(\gamma-1)]V(dp/d\theta)$. Because the settings for pressure pegging, filtering, TDC alignment, γ treatment, cycle count, and the raw pressure files were not retained, the supplied p-θ/HRR curves are used comparatively rather than reprocessed. Indicated thermal efficiency would require $\eta_i = W_{i,n}/(mf\ LHV)$; cycle-resolved fuel mass or a calibrated fuel-flow rate was unavailable, so no thermal-efficiency curve is reported. The experiment comprised four methanol concentrations (M = 0, 5, 10, and 15 vol.%) and six engine speeds (N = 1500-4000 rpm in 500-rpm increments), yielding 24 measured conditions. Although the original analysis framework specified the second-order response surface $Y = \beta_0 + \beta_1 M + \beta_2 N + \beta_{12} MN + \beta_{11} M^2 + \beta_{22} N^2 + \varepsilon$, the retained archive does not contain the regression coefficients, ANOVA/lack-of-fit output, residual diagnostics, desirability bounds/weights, or independent confirmation runs. Therefore, no inferential significance, predictive accuracy, absolute desirability, or statistically validated optimum is claimed; statistical interpretation is restricted to descriptive comparisons supported by the measured matrix.

Table 3. Experimental factors, response definitions, and interpretation scope

Category	Factor / response	Levels or definition	Interpretation scope
Factor	Methanol fraction, M	0, 5, 10, 15 vol.%	Measured factor
Factor	Engine speed, N	1500-4000 rpm; 500-rpm interval	Measured factor
Combustion	Pmax; CA10; CA50; CA90; BD	BD = CA90 − CA10	Combustion-phasing diagnostic

© The Author(s)
Published by Universitas Negeri Padang.
This is an open-access article under the: https://creativecommons.org/licenses/by/4.0/

Category	Factor / response	Levels or definition	Interpretation scope
Performance	$W_{i,n}$; $IMEP_n$	Cycle-integrated work; $W_{i,n}/Vd$	Descriptive indicated-performance response
Stability	COVIMEP	100 σIMEP / mean IMEP	Within-run cyclic-variability response
Emissions	CO; HC	Measured exhaust concentrations	Descriptive incomplete-combustion response
Mixture/exhaust	CO_2; O_2; λ; AFR	Measured / instrument-derived	Supporting mixture/exhaust indicators

3. Results and discussion

3.1 Fuel characteristics

The archived laboratory sheet reports a slight density increase from 786.02 kg/m³ for PWPO to 786.89 kg/m³ for M15, a kinematic-viscosity decrease from 0.879 to 0.821 cSt, and a research-octane-number increase from 71.6 to 84.5. The source sheet contains one reported value per fuel-property entry and does not retain replicate-level measurements, the number of repeats, or standard deviations. Table 4 is therefore presented as a descriptive property dataset without fabricated error bars or inferential statistics.

Table 4. Physicochemical properties of PWPO and methanol blends

Parameter	Sample				Test Method/ Standard
	PWPO	M5	M10	M15	
Density (kg/m³)	786.02	786.31	786.60	786.89	SNI 3506:2017
Kinematic viscosity at 40 °C (cSt)	0.879	0.859	0.840	0.821	
Initial Boiling point (°C)	43.4	44.5	45.8	47.0	
Flash point (°C)	50.9	44	38	33	
Gross (higher) heating value, HHV (MJ/kg)	42.156	41.176	40.198	39.219	ASTM D4809-06
Research octane number	71.6	77.0	81.0	84.5	ASTM D2699

Collectively, the results presented in Table 4 show that methanol reformulation introduces competing changes in fuel properties. From PWPO to M15, kinematic viscosity decreases by approximately 6.6%, and research octane number rises from 71.6 to 84.5; these changes support easier mixture preparation and greater resistance to autoignition in SI operation. At the same time, gross heating value decreases by nearly 7.0% and flash point decreases from 50.9 to 33°C, while the modest increase in initial boiling point shows that multicomponent volatility cannot be represented by flash point alone. These measured property trends provide a physically plausible context for the subsequent non-monotonic combustion response: improved oxygenation/mixture preparation may compete with reduced energy density and methanol-induced evaporative cooling [11], [12]. Because quantitative composition, fuel flow, and charge-temperature data are unavailable, this linkage is interpreted as a mechanism-consistent explanation rather than direct causal proof.

© The Author(s)
Published by Universitas Negeri Padang.
This is an open-access article under the: https://creativecommons.org/licenses/by/4.0/

3.2 Combustion performance

3.2.1 Peak cylinder pressure and pressure-volume behavior

Figures 2 and 3 present pressure-volume (P-V) behavior and maximum cylinder pressure over the speed sweep. The larger enclosed P-V loops at higher speeds correspond to greater indicated work, while M10 generally gives the strongest pressure development among the PWPO-based fuels. These P-V plots should not be described as pressure-crank-angle traces: volume is not a substitute for crank angle when locating peak pressure relative to TDC.

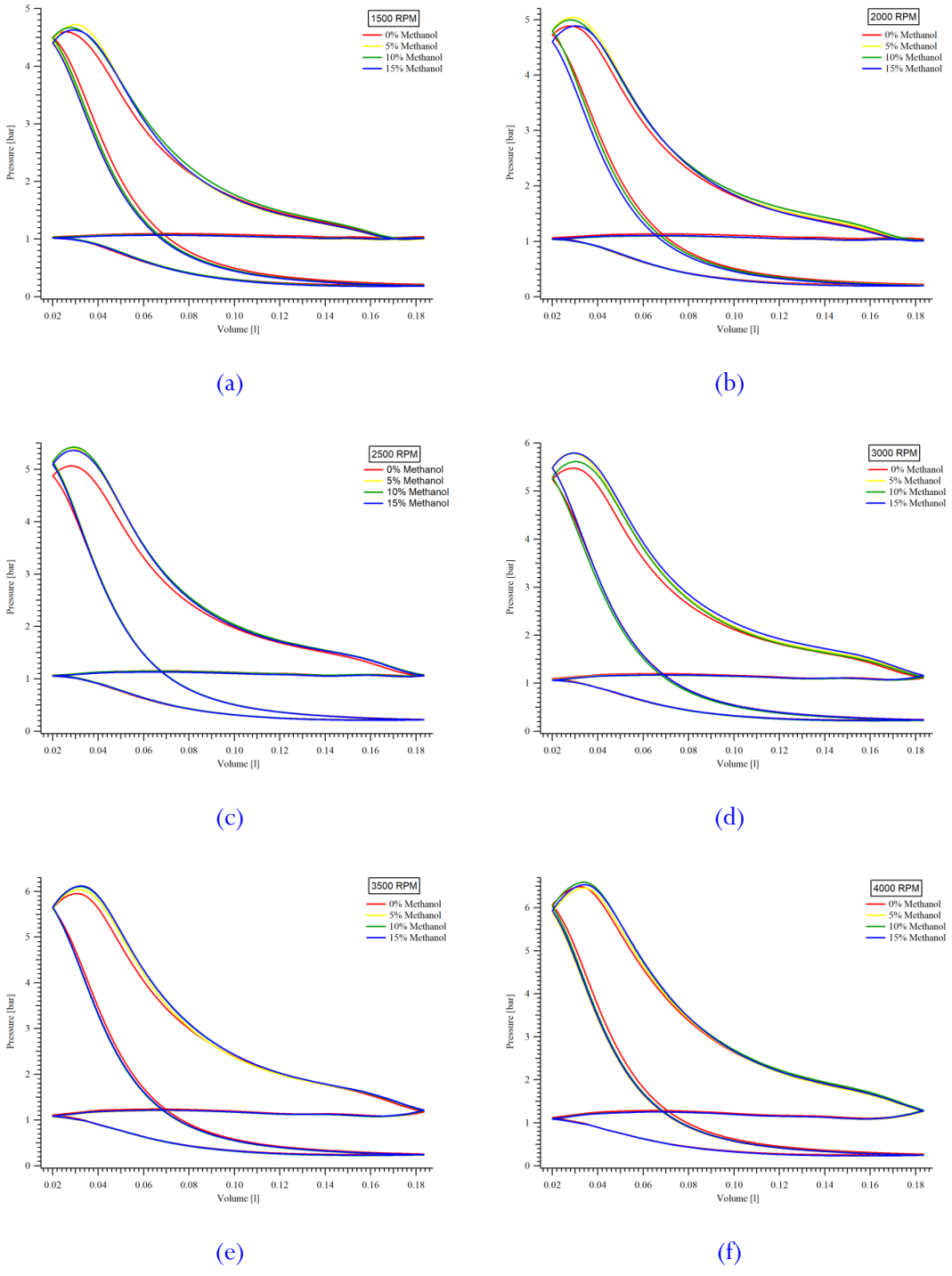


Figure 2. Cylinder pressure-volume diagrams for PWPO, M5, M10, and M15 at (a) 1500, (b) 2000, (c) 2500, (d) 3000, (e) 3500, and (f) 4000 rpm

© The Author(s)
Published by Universitas Negeri Padang.
This is an open-access article under the: https://creativecommons.org/licenses/by/4.0/

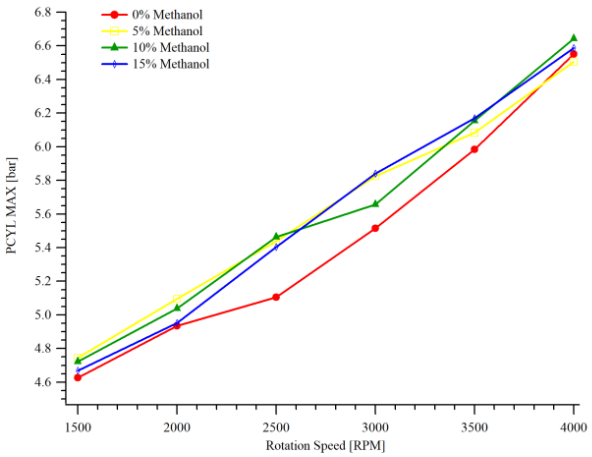


Figure 3. Maximum cylinder pressure as a function of engine speed and methanol fraction

3.2.2 Pressure-crank-angle and apparent heat-release rate

Figure 4 presents the cylinder-pressure and apparent HRR histories for all four fuels at 1500, 2000, 2500, 3000, 3500, and 4000 rpm. The pressure traces rise through compression and peak shortly after TDC, while the HRR curves develop a broad main-burn maximum during early expansion. Across the speed sweep, the peak-pressure range increases from approximately 4.6-4.8 bar at 1500 rpm to about 6.5-6.6 bar at 4000 rpm, consistent with the P-V and Pmax trends in Figures 2 and 3.

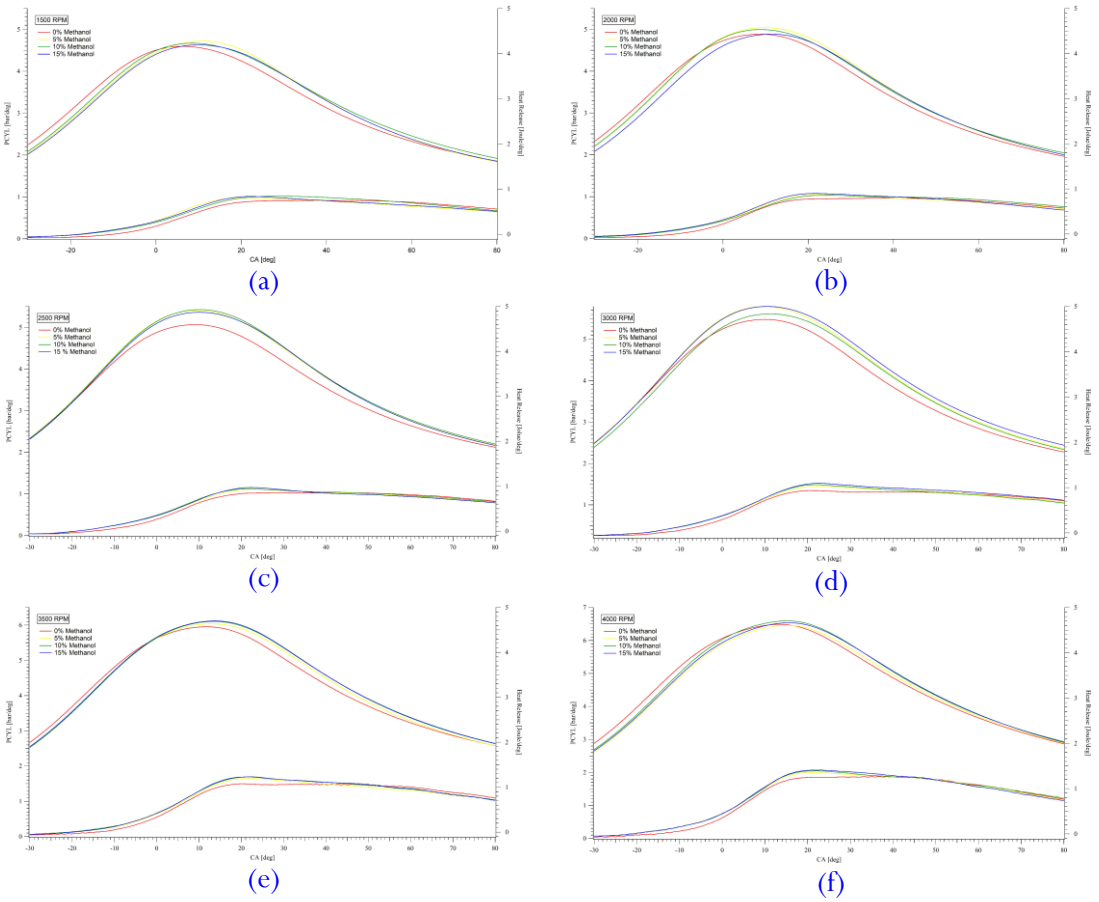


Figure 4. Cylinder pressure (PCYL) and apparent heat-release rate (HRR) versus crank angle for PWPO and 5, 10, and 15 vol.% methanol blends at (a) 1500, (b) 2000, (c) 2500, (d) 3000, (e) 3500, and (f) 4000 rpm

© The Author(s)
Published by Universitas Negeri Padang.
This is an open-access article under the: https://creativecommons.org/licenses/by/4.0/

© The Author(s)
Published by Universitas Negeri Padang.
This is an open-access article under the: https://creativecommons.org/licenses/by/4.0/

The blend ordering is not monotonic. At 1500-2000 rpm, the pressure curves remain closely grouped, and M5 can equal or slightly exceed M10 near peak pressure, whereas the HRR maxima differ only modestly. From roughly 2500 rpm upward, the oxygenated blends generally occupy the upper part of the main-burn pressure/HRR envelope relative to neat PWPO, with M10 and M15 most prominent at 3500-4000 rpm. Thus, the observed effect is a moderate shift in main-burn amplitude and phasing rather than a concentration-proportional increase. This pattern is consistent with competing oxygenation/mixture-preparation benefits and evaporative charge cooling, but those mechanisms are not directly quantified here because charge temperature and detailed fuel composition were not measured in the retained dataset [14], [15]. The p-θ/HRR evidence also resolves the apparent conflict between earlier CA90 and the longer CA10-CA90 interval for M10: an earlier end of combustion can coexist with a longer interval when CA10 advances by a larger amount. Accordingly, burn duration is interpreted together with pressure and HRR phasing, not as an isolated efficiency surrogate. The lower CO and HC measured for the methanol blends support reduced incomplete oxidation at selected conditions, but the HRR curves alone do not establish thermal efficiency without fuel-consumption data.

3.2.3 Combustion phasing and duration

Figure 5 shows that M10 advances both CA10 and CA90 relative to neat PWPO, with the larger advance occurring at CA10; consequently, the CA10-CA90 interval was approximately 2.8-5.6% longer across the tested speeds. At 3000 rpm, for example, the plotted interval is about 74.5°CA for M10 and 72.5°CA for PWPO. These are directly observable phasing differences. Their efficiency implication is not assumed: an earlier CA90 may reduce late expansion-stroke oxidation, but combustion duration alone cannot establish higher efficiency or more complete combustion. Any mechanistic interpretation must therefore be checked against the pressure-derived HRR, indicated work, COVIMEP, and measured emissions rather than inferred from CA10-CA90 in isolation.

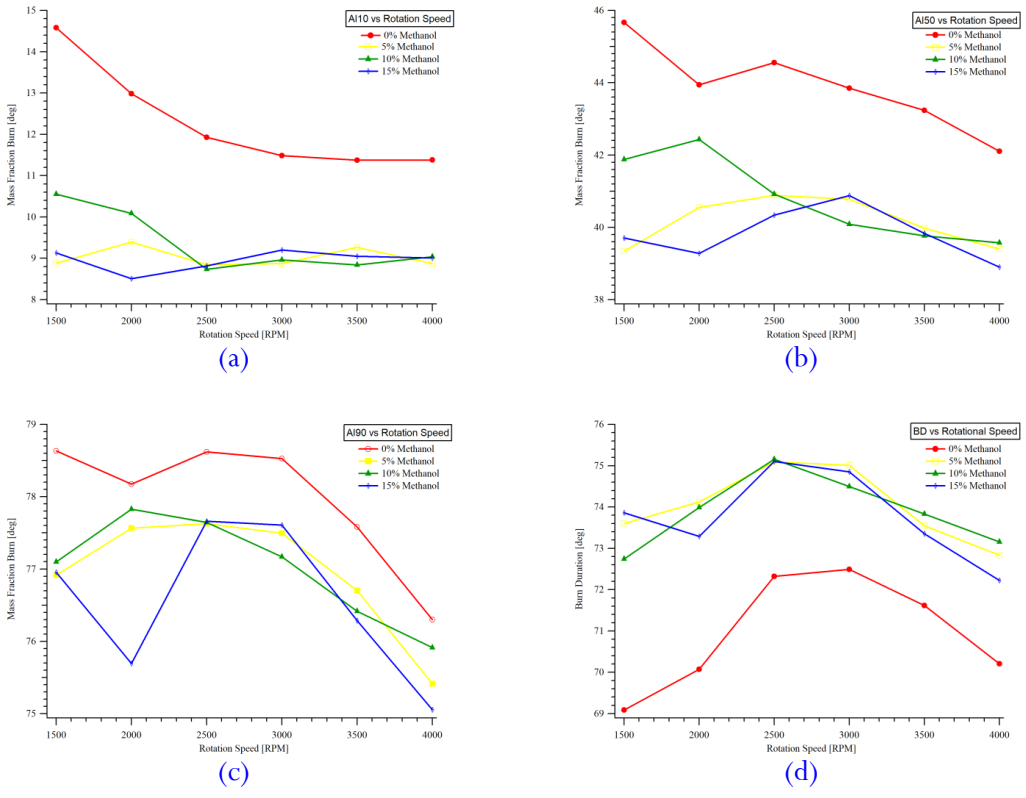


Figure 5. Effect of engine speed and methanol fraction on (a) CA10, (b) CA50, (c) CA90, and (d) CA10-CA90 burn duration

3.2.4 Indicated performance and combustion stability

Figures 6-8 show that $IMEP_n$, indicated work, and COVIMEP respond differently to methanol fraction and speed. M10 generally gives the highest $IMEP_n$ and indicated work among the PWPO-based fuels, but the COVIMEP values remain high under the present no-load condition. For M10, COVIMEP is approximately 16-25% across the tested speeds, indicating substantial cycle-to-cycle dispersion in these no-load tests. Thus, an improvement in mean work should not be interpreted as evidence of acceptable combustion stability. The rise of both $IMEP_n$ and indicated work with speed is not independent evidence because $IMEP_n = W_{i,n}/Vd$. The parallel trends simply reflect the same increase in enclosed P-V loop area normalized by displacement. In a mechanically governed carbureted engine, changes in admitted mixture and turbulence may contribute to the larger loops at higher speed, but this remains conditional because throttle position, air flow, and fuel flow were not reported. The data therefore support a speed-dependent indicated response, not a universal statement that higher speed intrinsically improves efficiency.

The blend response is also non-monotonic. M5 shows improvement in selected responses, whereas M10 shows the strongest mean indicated response among the tested blends. This pattern is consistent with a balance between improved oxygen availability/mixture preparation and the counteracting charge-cooling penalty of additional methanol [14], [15]. The supplied p-θ/HRR plots support this interpretation qualitatively; however, the missing raw cycle files, complete Kistler processing metadata, and fuel-flow data prevent a cycle-resolved uncertainty analysis or attribution of changes in thermal efficiency. Indicated thermal efficiency cannot be determined reliably from IMEP or indicated work alone. It requires cycle-resolved fuel mass (or a calibrated fuel-flow rate mapped to cycles) and the corresponding LHV. Because these inputs were unavailable, no inferred thermal-efficiency curve is reported.

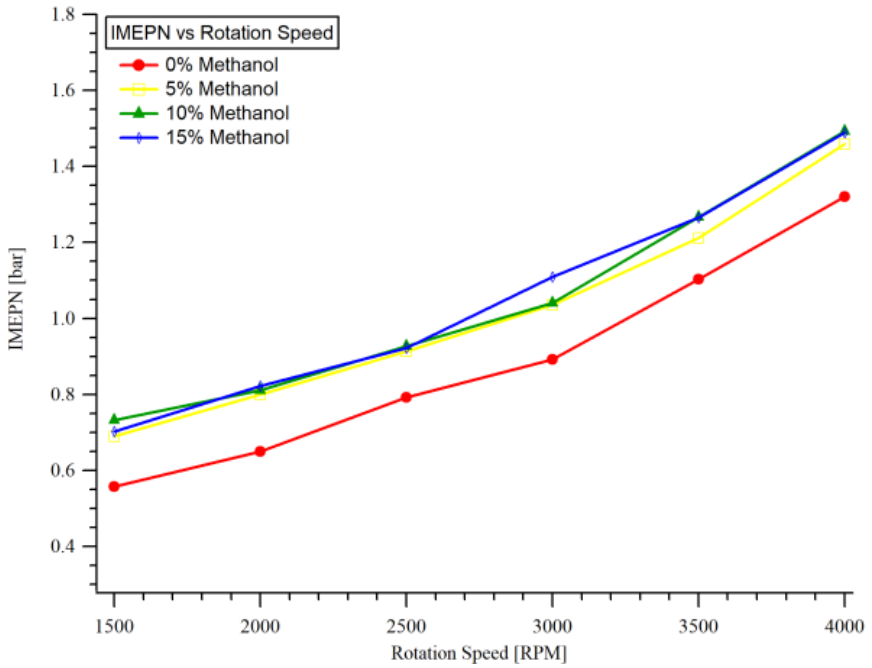


Figure 6. Net indicated mean effective pressure ($IMEP_n$)

© The Author(s)
Published by Universitas Negeri Padang.
This is an open-access article under the: https://creativecommons.org/licenses/by/4.0/

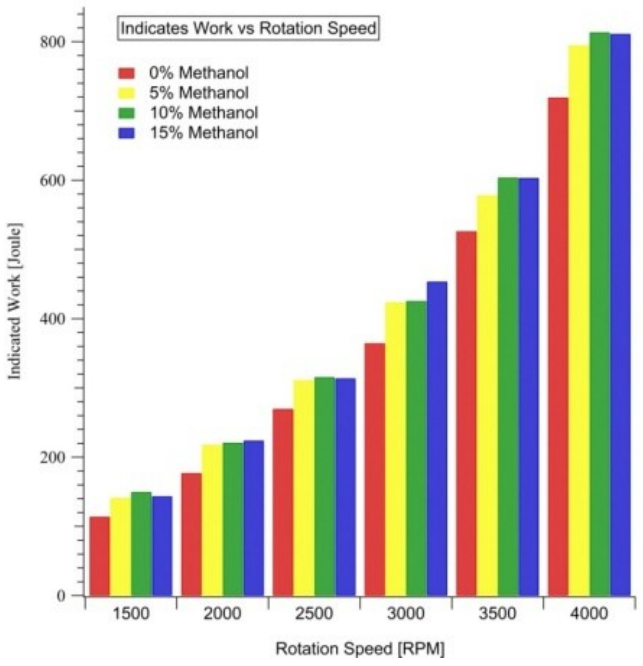


Figure 7. Indicated work, IW

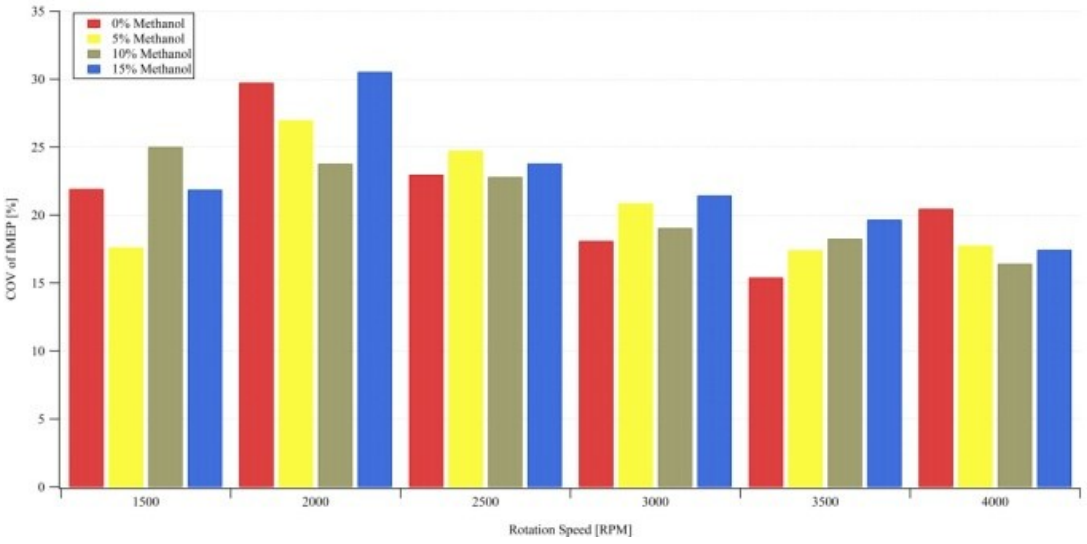


Figure 8. Coefficient of variation of net indicated mean effective pressure (COVIMEP)

3.2.5 Statistical scope, repeatability, and reproducibility

The retained manuscript and analysis package were audited for regression coefficients, ANOVA/lack-of-fit, residual diagnostics, response-specific desirability settings, confirmation runs, replicate-level engine measurements, and cycle-count metadata. These records were not recoverable. Accordingly, no confidence intervals, repeat-run error bars, desirability surface, parity plot, unsupported numerical desirability claim, model-accuracy claim, robustness claim, or statistically validated optimum is reported. The reported COVIMEP values characterize cycle-to-cycle dispersion within the archived combustion analysis and must not be interpreted as experimental repeatability across independent runs. The 24-condition matrix therefore supports descriptive ranking only: M10 and the intermediate-speed region may be identified as the most favorable tested compromise for selected responses, but not as a global or statistically validated optimum.

© The Author(s)
Published by Universitas Negeri Padang.
This is an open-access article under the: https://creativecommons.org/licenses/by/4.0/

3.2.6 Emission analysis

Figures 9-10 and Table 5 show a non-monotonic emission response to methanol. Averaged over the six tested speeds, CO decreased from 4.65 vol.% for PWPO to 3.87 vol.% for M5 (−16.9%), 3.99 vol.% for M10 (−14.2%), and 4.25 vol.% for M15 (−8.7%). Speed-averaged HC decreases from 572.3 ppm for PWPO to 441.5 ppm for M5 (−22.9%), 411.7 ppm for M10 (−28.1%), and 523.8 ppm for M15 (−8.5%). Thus, M5 gives the lowest mean CO, whereas M10 gives the lowest mean HC; no single tested methanol fraction yielded the lowest mean value for both pollutants. At 1500-2000 rpm, M15 still exhibits 717 ppm HC at 1,500 rpm and 677 ppm HC at 2,000 rpm and reaches $\lambda = 1.712$ at 2,000 rpm, demonstrating that additional methanol does not guarantee lower incomplete-combustion emissions. The pattern is consistent with a competition between oxygen-assisted oxidation/mixture preparation and charge-cooling or flame-development penalties, but this remains a mechanism-consistent interpretation rather than direct causal proof. CO_2, O_2, λ, and AFR are therefore used only as supporting mixture indicators. Table 6 summarizes the descriptive speed-averaged emission differences; no inferential statistics are attached because independent repeat-run data were not retained.

Taken together, the emission and combustion evidence identifies a trade-off rather than a single pollutant optimum. M5 provides the largest mean CO reduction, while M10 combines the largest mean HC reduction with the strongest indicated response overall. This is why M10 is described as the best tested multi-response compromise rather than the statistically validated optimum. The interpretation remains bounded by the high no-load COVIMEP, missing raw cycle-processing metadata, and absence of fuel-flow measurements, which preclude claims of universally stable or more thermally efficient operation.

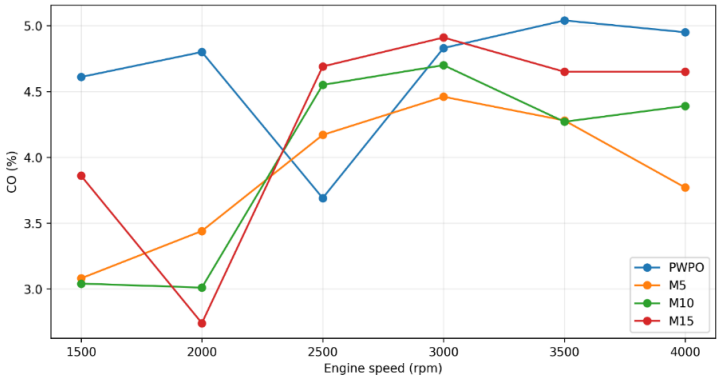


Figure 9. Carbon monoxide emissions as a function of engine speed and methanol fraction

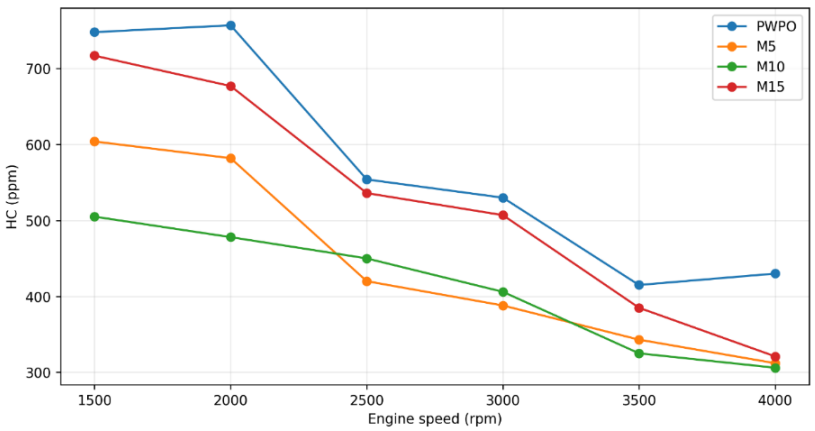


Figure 10. Unburned hydrocarbon emissions as a function of engine speed and methanol fraction

© The Author(s)
Published by Universitas Negeri Padang.
This is an open-access article under the: https://creativecommons.org/licenses/by/4.0/

Table 5. Exhaust-gas emissions and mixture indicators for PWPO and methanol blends

PWPO (vol.%) : methanol (vol.%)	Engine speed	CO (%)	HC (ppm)	CO_2 (%)	O_2 (%)	Lambda (λ)	AFR
100 : 0 (PWPO)	1500	4.61	748	5.10	7.15	1.219	17.90
	2000	4.80	757	5.30	6.78	1.178	17.30
	2500	3.69	554	5.10	6.89	1.289	18.90
	3000	4.83	530	6.10	5.38	1.095	16.10
	3500	5.04	415	6.50	4.48	1.036	15.20
	4000	4.95	430	7.00	3.76	0.998	14.60
95 : 5 (M5)	1500	3.08	604	5.50	8.19	1.426	20.90
	2000	3.44	582	5.80	7.26	1.314	19.30
	2500	4.17	420	6.00	6.13	1.190	17.40
	3000	4.46	388	6.30	5.31	1.118	16.40
	3500	4.28	343	6.40	4.87	1.102	16.20
	4000	3.77	312	7.20	4.41	1.097	16.10
90 : 10 (M10)	1500	3.04	505	5.40	8.36	1.457	21.40
	2000	3.01	478	5.90	7.7	1.390	20.40
	2500	4.55	450	5.50	6.41	1.188	17.40
	3000	4.70	406	5.90	5.58	1.123	16.50
	3500	4.27	325	6.20	5.01	1.114	16.30
	4000	4.39	306	7.20	4.18	1.053	15.40
85 : 15 (M15)	1500	3.86	717	5.50	7.3	1.280	18.80
	2000	2.74	677	4.30	10.23	1.712	25.10
	2500	4.69	536	5.80	6.13	1.152	16.90
	3000	4.91	507	5.90	5.47	1.099	16.10
	3500	4.65	385	6.30	4.88	1.081	15.90
	4000	4.65	321	6.70	4.38	1.053	15.40

Table 6. Speed-averaged CO and HC across the six tested engine speeds

Fuel	Mean CO (vol.%)	ΔCO vs PWPO (%)	Mean HC (ppm)	ΔHC vs PWPO (%)
PWPO	4.65	0.0	572.3	0.0
M5	3.87	−16.9	441.5	−22.9
M10	3.99	−14.2	411.7	−28.1
M15	4.25	−8.7	523.8	−8.5

Note: Values are descriptive arithmetic means across 1500-4000 rpm. They do not represent repeat-run means or inferential estimates because replicate-level engine-test data were not retained.

3.3 Comparative discussion with previous studies

The contribution becomes clearer when the complete evidence chain is considered. Previous engine studies have investigated valve timing, EGR, and fuel-injection strategies to improve performance and emissions [20], [21], [22], [23]; the present contribution instead lies in coupling fuel-property changes with crank-angle-resolved combustion, indicated response, cyclic variability, and emissions under one PWPO-methanol matrix. Measured viscosity and heating-value changes provide the property boundary; p-θ/HRR and CA10-CA90 establish that the main-burn response shifts non-

© The Author(s)
Published by Universitas Negeri Padang.
This is an open-access article under the: https://creativecommons.org/licenses/by/4.0/

monotonically; $IMEP_n$ indicates that M10 generally gives the strongest mean indicated response; and COVIMEP shows that this gain does not imply conventional cycle stability [24], [25], [26], [27], [28]. The emission data add a further trade-off: M5 yields the lowest speed-averaged CO, whereas M10 yields the lowest HC and a stronger indicated response. This separation among responses is precisely why the result should not be reduced to a single 'optimum' blend. Mechanistically, these observations align with competition between oxygen-assisted oxidation/mixture preparation and evaporative cooling in alcohol-containing SI fuels [12], [13]. PWPO studies separately identify sensitivity to feedstock, cracking severity, and fuel-property distribution [6], [7]. Other combustion studies involving different fuels and engine architectures are considered only as contextual comparisons [29], [30]. Because quantitative GC-MS fractions, charge-temperature data, calibrated fuel flow, complete pressure-processing metadata, and independent repeat-run statistics are unavailable, these mechanisms are presented as bounded interpretations of measured trends, not as directly proven causal pathways.

4. Conclusion

This study evaluated catalytic PWPO containing 0-15 vol.% methanol in a 163 cm^3 single-cylinder stationary Otto engine at 1,500-4,000 rpm. The p-θ/HRR data showed pressure maxima shortly after TDC and broad main-burn heat release during early expansion, with a non-monotonic response to methanol. M10 generally produced the highest $IMEP_n$. In contrast, M5 yielded the lowest speed-averaged CO (3.87 vol.%, −16.9% relative to PWPO), whereas M10 produced the lowest HC (411.7 ppm, −28.1%) and a 14.2% CO reduction. M10 did not shorten CA10-CA90: its interval was approximately 2.8-5.6% longer than PWPO despite earlier CA90, and its COVIMEP remained approximately 16-25% under the no-load condition. These results show that mean indicated response, burn phasing, cyclic variability, and emissions do not improve monotonically or simultaneously as the methanol fraction increases.

Scientific contribution and interpretation. The study's contribution is the integrated demonstration of this multi-response trade-off for catalyst-derived PWPO-methanol fuel in a stationary SI-engine setting, rather than the mere use of methanol or a model-derived optimum. M10 is therefore described only as the best tested multi-response compromise within the measured domain, not as a statistically validated or globally optimal blend. The property-to-combustion explanation is consistent with competing mixture/oxygenation benefits and methanol-related charge cooling, but remains interpretive because quantitative composition, charge temperature, raw cycle files, complete processing metadata, calibrated fuel flow, and independent repeat-run statistics were not retained. Future validation should prioritize loaded constant-speed operation, cycle-resolved pressure reprocessing with documented TDC/pegging/filtering settings, calibrated fuel-flow measurement, quantitative GC-MS supported by calibration and documented peak assignments, separately documented FTIR characterization, phase-stability testing, catalyst characterization, and a complete uncertainty and repeatability analysis.

Author's declaration

Author contribution

Enzo Wiranta Battra Siahaan: Writing - original draft, Methodology, Investigation, Formal analysis, Conceptualization. **Tulus Burhanuddin Sitorus:** Writing - original draft, Methodology, Investigation, Formal analysis, Conceptualization. **Himsar Ambarita:** Writing - Review & Editing, Visualization, Resources, Methodology. **Taufiq Bin Nur:** Writing - Review & Editing, Methodology. **Ilmi Abdullah:** Writing - Review & Editing, Methodology, Data curation, Conceptualization. **Janter P. Simanjuntak:** Writing–review & editing, Validation, Supervision, Conceptualization.

© The Author(s)
Published by Universitas Negeri Padang.
This is an open-access article under the: https://creativecommons.org/licenses/by/4.0/

Funding statement

This research was funded by the Directorate of Research, Technology, and Community Service (DRTPM) under the Ministry of Education, Culture, Research, and Technology of the Republic of Indonesia, with contract No. 02/UN5.4.10.K/PT.01.03/KP-DPPM/2025.

Data availability

The retained data supporting the reported 24-condition matrix are available from the corresponding author upon reasonable request. Raw cycle files and complete combustion-processing metadata were not retained and are therefore not represented as available.

Acknowledgements

The authors would like to express their sincere gratitude to the Directorate of Research, Technology, and Community Service (DRTPM), under the Ministry of Education, Culture, Research, and Technology of the Republic of Indonesia, for providing financial support through the Doctoral Dissertation Research Grant.

Conflict of interest

The authors declare that they have no known competing financial interests or personal relationships that could have appeared to influence the work reported in this paper.

Ethical clearance

Not applicable

AI statement

ChatGPT (OpenAI) was used only for language and editorial assistance during manuscript revision. The manuscript was also proofread by a qualified English language expert to ensure grammatical accuracy, clarity, and appropriate academic language. The authors manually verified the experimental data, calculations, figures, scientific interpretations, and references and accept full responsibility for the final manuscript.

Publisher's and Journal's note

Universitas Negeri Padang as the publisher, and Editor of Teknomekanik state that there is no conflict of interest towards this article publication.

References

[1] G. Garcia-Garcia, M. Á. Martín-Lara, M. Calero, and G. Blázquez, "Environmental impact of different scenarios for the pyrolysis of contaminated mixed plastic waste," *Green Chemistry*, vol. 26, no. 7, 2024, https://doi.org/10.1039/d3gc04396g

[2] A. B. Cuevas, D. E. Leiva-Candia, and M. P. Dorado, "An Overview of Pyrolysis as Waste Treatment to Produce Eco-Energy," *Energies* , vol. 17, no. 12. 2024. https://doi.org/10.3390/en17122852

[3] E. W. B. Siahaan, T. B. Sitorus, H. Ambarita, T. Bin Nur, Ilmi, and J. P. Simanjuntak, "Catalytic Pyrolysis of Plastic Waste for Gasoline Fuel: Reaction Mechanism Engine

© The Author(s)
Published by Universitas Negeri Padang.
This is an open-access article under the: https://creativecommons.org/licenses/by/4.0/

Integration," *Automotive Experiences*, vol. 8, no. 2. 2025. https://doi.org/10.31603/ae.13822

[4] J. P. Simanjuntak, M. Z. Zainon, N. W. B. M. Zulkifli, B. H. Tambunan, J. L. Sihombing, and Riduwan, "Development of an Innovative Thermal Cracking of Mixed-Plastic Waste Without Catalyst as an Alternative Fuel Source," *International Journal of Technology*, vol. 15, no. 5, 2024, https://doi.org/10.14716/ijtech.v15i5.6905

[5] D. Kim, J. Kim, Y. Son, and S. Park, "Characteristics of the in-cylinder flow and spray for intake valve timing in an optical GDI engine with spray-guided injection," *Energy*, vol. 307, 2024, https://doi.org/10.1016/j.energy.2024.132574

[6] S. H. Susilo, I. Mashudi, S. Santoso, A. Hardjito, and D. Pebrianti, "Power and Emission Estimation of Plastic Waste Pyrolysis-Derived Fuel Blends in Internal Combustion Engines," *Eastern-European Journal of Enterprise Technologies*, vol. 6, no. 10(132), 2024, https://doi.org/10.15587/1729-4061.2024.318593

[7] Z. Mufrodi *et al.*, "Investigation and characterization of polypropylene plastic waste pyrolysis oil: Effect of temperature and fractional condensation," *Journal of Ecological Engineering*, vol. 26, no. 1, 2025, https://doi.org/10.12911/22998993/195533

[8] T. Thoharudin, T. H. A. Santosa, and I. Iswandi, "Evaluation of Motorcycle Fueled with Blends of Gasoline and Pyrolytic Oil from Plastic–Palm Kernel Shell Co-Pyrolysis," *ROTASI*, vol. 27, no. 1, 2025, https://doi.org/10.14710/rotasi.27.1.15-22

[9] J. N. Cruz, I. P. Hernández, J. E. Franyutti, R. M. V. Espino, and E. A. Z. Cárdenas, "Plastic recycling for liquid fuel production and its use in thermal engines," *Ecological Engineering and Environmental Technology*, vol. 26, no. 5, 2025, https://doi.org/10.12912/27197050/202778

[10] S. Septarini, A. Amrullah, and C. A. Hakim, "Effect of phosphoric acid activation concentration on the proximate characteristics of municipal solid waste-derived biochar," *Innovation in Engineering*, vol. 3, no. 2, pp. 169–181, Sep. 2026, https://doi.org/10.58712/ie.v3i2.51

[11] X. Li, F. Xie, Y. Liu, X. Li, Y. Su, and Y. Zhou, "Study on the Influence of Different Internal Exhaust Gas Recirculation Formation Modes on the Combustion Performance of Gasoline, Methanol, and Ethanol SI Engine," *International Journal of Automotive Technology*, vol. 25, no. 3, 2024, https://doi.org/10.1007/s12239-024-00039-1

[12] M. Hanifuddin, M. F. Taufiqurrahman, T. A. Setyawan, R. Anggarani, C. S. Wibowo, and B. Sugiarto, "Performance of a Single-Cylinder Four-Stroke Engine with High Concentrations of Gasoline-Ethanol-Methanol (GEM)," *Automotive Experiences*, vol. 6, no. 2, 2023, https://doi.org/10.31603/ae.9332

[13] R. Meherzi, C. Boubahri, D. O. Lendoye, A. Elleuch, and J. Bessrour, "Numerical simulation of the effect of adding oxygenated fuel (ethanol) to commercial gasoline on engine performance and NOx emissions," *International Journal of Low-Carbon Technologies*, vol. 20, 2025, https://doi.org/10.1093/ijlct/ctae065

[14] Mokhtar, D. A. Sumarsono, A. A. Agama, A. Kurniawan, and H. Setiapraja, "Performance, Emissions, and Combustion Analysis of Gasoline-Ethanol-Methanol Blends in a Spark-Ignition Engine," *Results in Engineering*, vol. 26, 2025, https://doi.org/10.1016/j.rineng.2025.105264

[15] M. Gassoumi *et al.*, "Methanol as a fuel additive: effect on the performance and emissions of a gasoline engine," *Energy Sources, Part A: Recovery, Utilization and Environmental Effects*, vol. 45, no. 3, 2023, https://doi.org/10.1080/15567036.2023.2240741

[16] B. Waluyo, M. Setiyo, Saifudin, and I. N. G. Wardana, "Fuel performance for stable homogeneous gasoline-methanol-ethanol blends," *Fuel*, vol. 294, 2021, https://doi.org/10.1016/j.fuel.2021.120565

[17] M. Usman, S. M. M. A. Rizvi, M. S. Ali, F. Riaz, M. Saeed, and E. M. Abo-Zahhad, "Multi-objective prediction and optimization of alcohol–gasoline SI engines using a hybrid gradient

© The Author(s)
Published by Universitas Negeri Padang.
This is an open-access article under the: https://creativecommons.org/licenses/by/4.0/

boosting and evolutionary algorithm framework," *Results in Engineering*, vol. 30, 2026, https://doi.org/10.1016/j.rineng.2026.110203

[18] P. Paramasivam and D. C, "Multi-objective optimization of CRDI engine parameters fueled with blends of diesel and sterculia foetida biodiesel: A comparative study of RSM composite desirability and meta-heuristic algorithm," *Results in Engineering*, vol. 29, 2026, https://doi.org/10.1016/j.rineng.2026.109719

[19] F. J. Passamonti, V. M. Benitez, C. Especel, F. Epron, C. L. Pieck, and S. A. D'Ippolito, "SiO2-Al2O3 catalysts for methanol to olefins: Comparative study with SAPO34 and ZSM5," *Applied Catalysis A: General*, vol. 670, 2024, https://doi.org/10.1016/j.apcata.2023.119556

[20] Y. Wang, J. Tian, Y. Xiong, L. Wang, S. Ji, and Y. Cheng, "Optimization study on fuel injection characteristics of gasoline direct injection (GDI) engine fuel system," *Fuel*, vol. 381, 2025, https://doi.org/10.1016/j.fuel.2024.133468

[21] M. Mohamed, A. Biswal, X. Wang, H. Zhao, and J. Hall, "Experimental investigation for enhancing the performance of hydrogen direct injection compared to gasoline in spark ignition engine through valve timings and overlap optimization," *Fuel*, vol. 372, 2024, https://doi.org/10.1016/j.fuel.2024.132257

[22] R. Novella, J. Gomez-Soriano, D. González-Domínguez, and O. Olaciregui, "Optimizing hydrogen spark-ignition engine performance and pollutants by combining VVT and EGR strategies through numerical simulation," *Applied Energy*, vol. 376, 2024, https://doi.org/10.1016/j.apenergy.2024.124307

[23] F. yu Lai *et al.*, "Experimental analysis and optimization of the variable valve timing on attaining high efficiency with low NOx emission of a direct-injected hydrogen engine," *Fuel*, vol. 381, 2025, https://doi.org/10.1016/j.fuel.2024.133199

[24] T. Tahtouh, M. André, G. Castellano, L. Rolando, and F. Millo, "A path toward a new generation of sustainable spark ignition engines: Experimental investigations on the synergic use of dual diluted combustion and renewable fuels," *Transportation Engineering*, vol. 20, 2025, https://doi.org/10.1016/j.treng.2025.100317

[25] S. Sahoo and D. K. Srivastava, "Effect of injection timing on combustion and IMEP variation of a bi-fuel compressed natural gas SI engine," *Environmental Progress and Sustainable Energy*, vol. 40, no. 6, 2021, https://doi.org/10.1002/ep.13694

[26] M. V. Mane and N. S. Solke, "Combustion thermodynamics in internal combustion engines: Performance, emission, and sustainability perspectives," *Chemical Thermodynamics and Thermal Analysis*, vol. 23. 2026. https://doi.org/10.1016/j.ctta.2026.100356

[27] Z. Zheng, P. Lappas, A. M. Shamekhi, X. Wang, and M. Mikulski, "Advancements in detecting combustion events through vibration analysis in internal combustion engines: a literature review," *Mechanical Systems and Signal Processing*, vol. 241. 2025. https://doi.org/10.1016/j.ymssp.2025.113539

[28] Z. Liu, Z. Zhang, S. Rao, and Z. Zheng, "Study of water injection on suppressing knock in a high compression ratio and supercharged hybrid gasoline engine," *Energy*, vol. 287, 2024, https://doi.org/10.1016/j.energy.2023.129702

[29] C. Woo, S. Kook, E. R. Hawkes, P. L. Rogers, and C. Marquis, "Dependency of engine combustion on blending ratio variations of lipase-catalysed coconut oil biodiesel and petroleum diesel," *Fuel*, vol. 169, 2016, https://doi.org/10.1016/j.fuel.2015.12.024

[30] A. V. Kale and A. Krishnasamy, "Experimental study on combustion, performance, and emission characteristics of a homogeneous charge compression ignition engine fuelled with multiple biofuel-gasoline blends," *Energy*, vol. 288, 2024, https://doi.org/10.1016/j.energy.2023.129621

© The Author(s)
Published by Universitas Negeri Padang.
This is an open-access article under the: https://creativecommons.org/licenses/by/4.0/

Nomenclature

$IMEP_n$	: Net indicated mean effective pressure
COVIMEP	: Coefficient of variation of IMEP
CO	: Carbon monoxide
HC	: Hydrocarbons
CO_2	: Carbon dioxide
O_2	: Oxygen
AFR	: Air-fuel ratio
BD	: Burn duration (CA90 − CA10)
HHV	: Higher heating value (MJ/kg)
HRR	: Heat-release rate
M	: Methanol fraction (vol.%)
N	: Engine speed (rpm)

© The Author(s)
Published by Universitas Negeri Padang.
This is an open-access article under the: https://creativecommons.org/licenses/by/4.0/